Model validation of a packed bed LTA membrane reactor for the direct synthesis of DME from CO/CO_2

Ainara Ateka*, Pablo Rodriguez-Vega, Tomás Cordero-Lanzac, Javier Bilbao, Andrés T. Aguayo

Department of Chemical Engineering, University of the Basque Country UPV/EHU, P.O. Box 644, 48080 Bilbao, Spain

*Corresponding author. Tel.: +34-94-6015361. E-mail address: ainara.ateka@ehu.eus

ABSTRACT

A model for simulating the direct synthesis of dimethyl ether (DME) in a packed bed membrane reactor (PBMR) has been validated, using a LTA zeolite hydrophilic membrane in a lab-scale reaction equipment. In the model, membrane permeability data and the kinetic model corresponding to a CuO-ZnO-ZrO_2/SAPO-11 catalyst have been used. Experimental runs have been carried out under the following conditions: 275-325 ºC; 20-40 bar; space time, 10 g h $(mol_C)^{-1}$; CO_2/CO_x ratio, 0, 0.5 and 1; H_2/CO_x ratio, 3. The model is suitable for predicting the molar fractions of the compounds of the reaction medium (H_2, CO, CO_2, H_2O, DME, methanol and hydrocarbons) in the reaction and permeate sections of the PBMR, and their evolution with time on stream. DME yield, CO and CO_2 conversions are greater in the PBMR than without using the membrane, due to the displacement of the thermodynamic equilibrium by the partial separation of H_2O from the reaction medium. For H_2+CO feeds, the maximum DME yield is 68% at 325 ºC and 40 bar with a space time value of 10 g h $(mol_C)^{-1}$. Otherwise, feeding H_2+CO_2, CO_2 conversion reaches 17%, with a DME yield over 5 %.

Keywords: DME synthesis, CO_2 valorization, membrane reactor, reactor simulation, hydrophilic membrane, LTA zeolite.

1. Introduction

Mitigating the serious environmental consequences of greenhouse gas emissions requires urgently developing effective technologies for the capture, storage and valorization of CO_2. The valorization routes receiving most attention are those directed to the production of methanol, dimethyl ether (DME), hydrocarbons (gasoline or olefins) and CH_4 [1-3]. The interest of these routes are related to the prospects for their large-scale technological development and the commercial interest of the products as fuels or raw materials, in a scenario in which replacing oil with other sources with greater availability (such as natural gas) and sustainability (biomass) is a priority.

The appeal of DME synthesis is based on its potential large-scale use as automotive and household fuel [4,5], and as a replacement for methanol as raw material for the production of hydrocarbons, especially light olefins [6-8]. The direct synthesis of DME by the hydrogenation of CO, CO_2 or a mixture of both, takes place on bifunctional catalysts through the following individual reactions:

Methanol synthesis: $$CO + 2H_2 \leftrightharpoons CH_3OH \quad (1)$$

$$CO_2 + 3H_2 \leftrightharpoons CH_3OH + H_2O \quad (2)$$

Methanol dehydration to DME: $$2CH_3OH \leftrightharpoons CH_3OCH_3 + H_2O \quad (3)$$

Water gas shift (WGS): $$CO + H_2O \leftrightharpoons CO_2 + H_2 \quad (4)$$

Hydrocarbons formation (undesired side reaction):

$$CO + 3H_2 \leftrightharpoons CH_4 + H_2O \quad (5)$$

Performing the dehydration of methanol (catalyzed by the acid function of the catalyst) *in situ*, in the same reactor, displaces the thermodynamic equilibrium of methanol

synthesis reactions (on the metallic function). The thermodynamic advantages of the direct synthesis of DME over methanol synthesis and over the conventional two-stage DME production process facilitate the conversion of CO_2 together with syngas and decrease the H_2 requirement in the feedstock, thus favoring the valorization of syngas derived from biomass [9-11]. The ideal reaction pressure and temperature conditions in the direct synthesis process are intermediate to the optimum for each individual reaction. Moreover, co-feeding CO_2 with *syngas* results in higher H_2O concentration in the reaction medium. These differences have urged to pay a great deal of attention to catalyst preparation, kinetic modeling, and reactor design [12-15]. The changes in the reaction medium composition when feeding CO_2 and the interactions between the two active functions of the catalyst are also features to be controlled in catalysts preparation. In this regard, the main challenge is to ensure the catalyst stability, by avoiding sintering and coke formation [16-19].

Kinetic models have been established for the new catalysts and conditions for the direct synthesis of DME. These models consider CO_2 co-feeding and catalyst deactivation [20,21]. And regarding the reactor configurations, packed bed reactors (PBR) have been mainly used because multitubular reactors are used industrially for the synthesis of methanol [22]. Considering the reaction scheme of the process (Eqs. (1)-(5)), the separation of H_2O from the reaction medium is a targeted objective aiming at reducing the thermodynamic limitations that condition the progress of methanol synthesis (Eqs. (1) and (2)) and its dehydration to DME (Eq. (3)). Besides, the concentration of H_2O has attenuating effects on the kinetics of these stages, as well as on the reverse WGS (reverse of Eq. (4)). This occurs because of the competitive adsorption of reactants and water on the active sites of the catalysts (metallic and acid) [23,24]. As aforementioned, the presence of H_2O also favors the sintering of the active sites of the CuO-ZnO

metallic function of the catalyst [25]. All in all, the implantation of a membrane in a packed bed reactor (PBMR) turns out as a more advanced technological solution in terms of scaling-up in comparison with other alternatives studied for the removal of H_2O from the reaction medium, such as reactive distillation [26] or *in situ* adsorption [27].

Zeolite membranes, with uniform pore size, high mechanical strength and chemical and thermal stability are the most suitable for operating above 200 ºC. Diban et al. [28] have reviewed the applications of zeolites with different crystalline structure (LTA, MFI, MOR, MER, PH, CHA) in the estherification of alcohol. Galluci et al. [29] have experimentally demonstrated the higher yield of methanol synthesis using a LTA membrane. Ferosov et al. [30] have used a LTA membrane (NaA Zeolite) for the dehydration of methanol towards DME reaching a methanol conversion of 88 % (80 % without membrane). And Gorbe et al. [31] have analyzed the capability of zeolite A for the separation of H_2O from H_2, CO_2 and H_2O mixtures, with the perspective of its future application in methanol synthesis, observing a remarkable limitation of this separation above 240 ºC.

Due to the constraints for the preparation of suitable membranes and their implementation in the reactor, the use of a PBMR in the direct synthesis of DME has only been studied by theoretical modeling and simulation. The membrane reactor simulation study of Iliuta et al. [32] is pioneer in considering CO_2 in the feed and quantifying the role of the membrane in order to favor the enhancement in methanol yield and DME selectivity. These authors have used the kinetics of a CuO-ZnO-Al_2O_3/HZSM-5 catalyst and considered the ideal situation where only H_2O and H_2 are affected by the membrane transport. Diban et al. [33] have proposed a more detailed

PBMR design model. They have used a kinetic model for a CuO-ZnO-Al_2O_3/γ-Al_2O_3 catalyst and studied the effect of the membrane transport properties (H_2O permeability and relative permeation selectivity of the compounds in the reaction medium) on the conversion of CO_2 and DME yield. These same authors [34] have also studied the effects of sweeping conditions, strategies and flowrates on the results. The simulation of de Falco et al. [35,36] considers: i) heat balance (different from previous models that consider isothermal reactors); ii) the kinetics of a CuO-ZnO-Al_2O_3/HZSM-5 catalyst and; iii) a CO_2 flow in the sweep stream (different from the previous models that consider the same H_2/CO_x ratio for sweeping and fed to the reaction section).

In this work, a model for the simulation of the direct DME synthesis process (STD process) in a packed bed membrane reactor (PBMR) using a hydrophilic LTA zeolite membrane has been validated with experimental runs using a LTA zeolite membrane. The main objective of this innovative reactor is the separation of H_2O from the reaction medium to favor the thermodynamic limitations of the process, especially relevant for CO_2 containing feedstocks, pursuing the enhancement of DME production and CO_2 conversion. In this way, the accuracy of the PBMR model leads not only to promising results in the direct synthesis of DME but also towards the fundamental design of PBMRs, targeting improvements in the membrane and operation conditions.

2. Experimental

2.1. Reaction and analysis equipment

The reaction equipment has been designed, built up and put into operation by modifying a commercial equipment for catalytic reactions (Microactivity Reference from PID Eng&Tech., Madrid, Spain). The feed gases enter the system through two sets of mass flow controllers (Bronkhorst High-Tech B.V. Series). The temperature is controlled and monitored by TOHO TTM-005 controllers and measured in both sections (reaction and permeation) by K-Type thermocouples. Two transducers (Sensor-Technik-Wiedemann GmbH) are used to control the pressure of the system. In turn, a small part of the reaction and permeate fluxes (around 1 cm^3) are diluted in a He stream and sent to the gas chromatograph (micro-GC Agilent 490) to be analyzed continuously in-line every 2.5 min. The micro-GC is provided with three analysis columns (molecular sieve, Porapak Q and Alumina), and further details of the analysis system have been described in detail elsewhere [16], [18], [37], [40]. A scheme of the packed bed membrane reactor (PBMR) is shown in Fig. 1. It consists of a stainless steel membrane tube (Mott Corporation), of 240 mm length (the catalytic bed takes 70 mm) and an inner diameter of 9.5 mm (number 3 in the scheme).

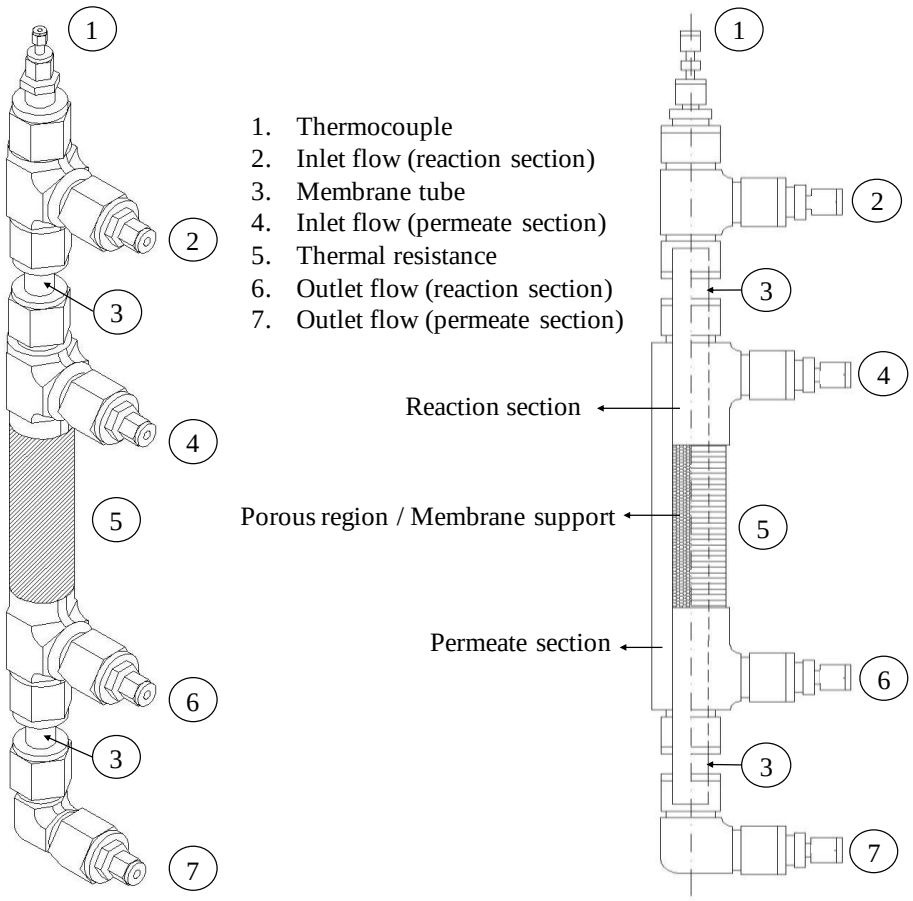

Fig. 1. Isometric and section view of the packed bed membrane reactor (PBMR).

2.2. Catalyst and membrane

The bifunctional CuO-ZnO-ZrO_2/SAPO-11 catalyst was prepared by dry physical mixture of the metallic and acid functions. The preparation of each of the functions has been optimized in previous works. From these studies the capacity of ZrO_2 for stabilizing the metallic function [37,38] and the selectivity and stability of SAPO-11 [39] are to be highlighted. A mass ratio of 1/2 between these two functions was used, as it has been determined to be the optimal [40]. The mixture was finely powdered, pelletized, crushed and sieved to 125-500 mm. The most relevant physic-chemical properties of each individual function and of the final catalyst are listed in Table S1. Prior to the experimental reactions, an *in situ* reduction of the catalyst with H_2 (diluted

in N_2) was carried out in the reactor at 250 ºC. The objective of this step is the complete reduction of the CuO species of the metallic function to Cu^0 and Cu^+, which are the active oxidation states for the hydrogenation of CO and CO_2 to methanol [41].

LTA zeolite was prepared adding a silicate solution into an aluminates solution under stirring at room temperature [42]. The resulting solution, with a molar ratio of 3.165 Na_2O:Al_2O_3:1.926 SiO_2:128 H_2O, was placed together with the stainless steel support (pore diameter 0.5 µm) in a horizontal Teflon-lined stainless steel autoclave (HighPreactor BR300, Berghoff) for the hydrothermal synthesis of the zeolite on the support. Once the LTA zeolite crystallized on the support (at 110 ºC for 12 h with a heating rate of 5 ºC min^{-1}), the membrane was washed with deionized water for several times, and then dried at room temperature for 24 h and calcined at 300 ºC before its characterization. From CO_2 adsorption analysis at 0 ºC, a micropore surface of 458 m^2 g^{-1} and a pore width of 3.98 Å are determined for the LTA membrane. The structure and appropriate crystallization on the support were confirmed by XRD tests. As to the permeation and thermal stability regards, the most relevant properties are gathered in Table 1 [43]. Let M_i be the mass of each i compound diffusing through the membrane of area A in a given time t. Then, Q_i is defined as the permeate flux through the membrane

$$Q_i = \frac{M_i}{A \cdot t}. \quad (6)$$

Besides, the separation factor achieved by the membrane of a binary mixture containing the compound i (α_i), in this case H_2O/ethanol or H_2O/methanol, is defined as the quotient between the ratio of the molar fractions of both compounds in the permeate (P) and in the reaction (R) section.

$$\alpha_i = \frac{(y_{H_2O}/y_i)_P}{(y_{H_2O}/y_i)_R} \quad (7)$$

where y_i is the molar fraction of ethanol or methanol.

Table 1. Pervaporation, vapor permeation and single gas permeation properties of the LTA membrane.

Technique	Temperature (ºC)	Composition	Feed (wt%)	Permeate (wt%)	Q_i (kg m^{-2} h^{-1})	α_i
PV	60	MeOH H_2O	90.0 10.0	0.75 99.2	1.05	1011
PV	75	EtOH H_2O	90.0 10.0	0.47 99.5	1.70	2905
VP	125	EtOH H_2O	90.0 10.0	0.19 99.8	1.32	3232

		Single gas permeation (10^{-9} mol m^{-2} s^{-1} Pa^{-1})				
		He	H_2	CO_2	N_2	CH_4
SGP	100	2.39	2.90	0.56	0.78	0.93
	150	3.47	4.60	0.94	1.24	1.61
	200	9.24	13.2	3.18	3.61	4.34

		Single gas permeation (10^{-9} mol m^{-2} s^{-1} Pa^{-1})					
		H_2	CO	CO_2	H_2O	MeOH	DME
SGP*	275	72	33	140	79	45	9.2
	325	73	33	141	81	50	23.1

PV: Pervaporation; VP: Vapor Permeation; SGP: Single Gas Permeation; SGP*: Single Gas Permeation feeding mixtures

The individual permeances of the *i* compounds present in the reaction medium were determined from real experimental values and permitted selecting the LTA membrane among others (LTX, SOD, MOR). The experiments were conducted using an inert (SiC) bed in the PBMR (that is, without catalyst) and the LTA membrane. After assessing gas

permeances individually (SGP) at 200 ºC, further tests were carried out under reaction temperature conditions, thus, at 275, 300 and 325 ºC (at 1.5 bar). The tests were performed using N_2 as sweeping gas in the permeate section while feeding the following compound mixtures in the same total flow rate (of 60 cm^3 min^{-1}): 1) H_2 (66 vol%), CO (17 vol%) and CO_2 (17 vol%); 2) H_2O (1 vol%), MeOH (9 vol%) and N_2 (90 vol%); 3) DME (78 vol%) and N_2 (22 vol%). The composition of each section (reaction and permeate) was analyzed in the micro-GC previously mentioned in section 2.1. As expected, the permeation of all compounds is favored with increasing temperature due to the enhanced diffusivity.

2.3. Reaction runs and indices

After the experimental runs using an inert bed for the characterization of the membrane, the catalyst was loaded in the reactor mixed with SiC in order to ensure isothermal conditions. After the reduction of the catalyst at 250 ºC (see section 2.2), the experimental runs were carried out at the following conditions: 275-325 ºC; 20-40 bar; space time of 10 g h $(mol_C)^{-1}$; CO_2/CO_x ratio of 0, 0.5 and 1; H_2/CO_x ratio, 3. Please note that in all cases, the same concentration of reactants is fed in the reactor and permeate sections of the PBMR in order to avoid the diffusion of these compounds through the membrane. Analogous runs were performed with a PBR configuration in order to compare the results and improvement of the PBMR. The reaction runs were monitored by following the yields of products and the conversion of the carbon reactants (CO and CO_2). Two different flows are analyzed at the outlet of a PBMR (reaction and permeate sections). The overall yield of each *i* product is then calculated

considering the total molar flow rates at the inlet and outlet of the reactor in terms of contained C units.

$$Y_i = \frac{n_i F_i}{F^0_{CO_x}} 100 \quad (8)$$

where n_i is the number of carbon atoms of each i product, F_i is the molar flow rate of the i product at the outlet of the PBMR and $F^0_{CO_x}$ the total molar flow rate of CO_x ($CO+CO_2$) in the feed.

CO_2 conversion is defined as:

$$X_{CO_2} = \frac{F^0_{CO_2} - F_{CO_2}}{F^0_{CO_2}} 100 \quad (9)$$

where $F^0_{CO_2}$ and F_{CO_2} are the molar flow rate of CO_2 at the inlet and outlet of the PBMR, respectively. This conversion is directly related with the capability of valorizing CO_2.

The conversion of CO_x is defined by the ratio between the moles of CO and CO_2 in the feed that have been converted:

$$X_{CO_x} = \frac{F^0_{CO_x} - F_{CO_x}}{F^0_{CO_x}} 100 \quad (10)$$

where F_{CO_x} is the molar flow of ($CO + CO_2$) at the outlet of the reactor.

3. Packed bed membrane reactor model description

3.1. General methodology

In the isothermal packed bed membrane reactor (PBMR), the permeances of the compounds from the reaction to the permeate section (and vice versa) needs to be taken into account. Therefore, the simulation of the PBMR is based on solving the

convection-dispersion equation for each *i* compound of the reaction medium. The flow geometry of the catalytic bed of the reactor is depicted in Fig. 2, where two concentric tubes are observed parallel to the *z* coordinate. The interphase between the tubes represents the LTA membrane, through which the compounds diffuse.

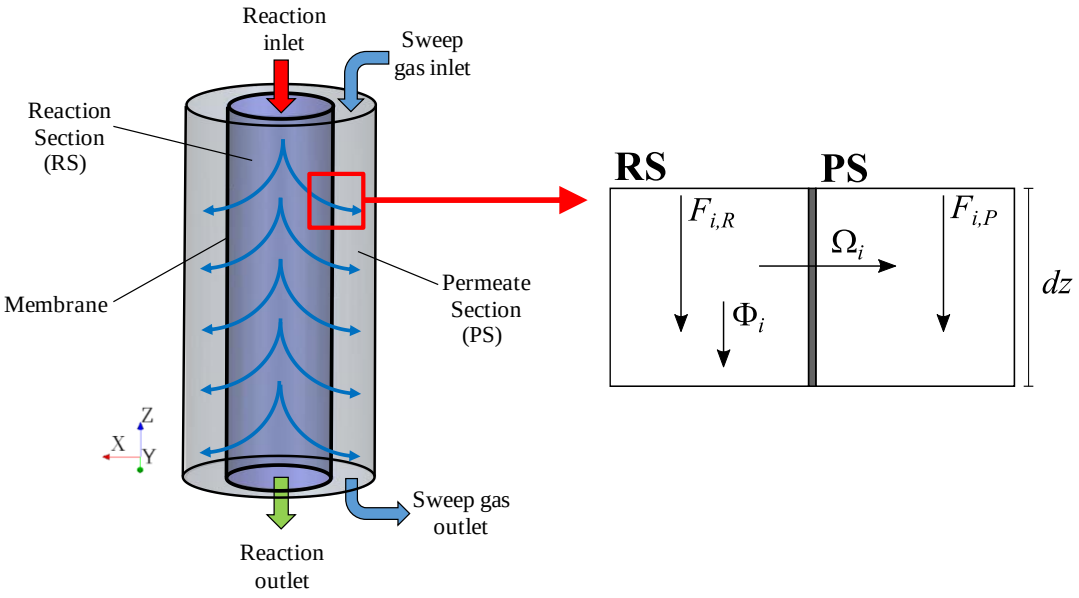

Fig. 2. Schematic geometry of the catalytic bed and description of the molar flows.

The one-dimension convection-dispersion equation for the concentration of each *i* compound (expressed in terms of partial pressure) in a porous catalytic bed can be written as:

$$\varepsilon \frac{\partial (P y_i)}{\partial t} = -\frac{\partial}{\partial z}\left[v P y_i - D \frac{\partial (P y_i)}{\partial z} \right] + s_i \tag{11}$$

where ε is the effective porosity of the bed, P is the total pressure, y_i is the molar fraction of each *i* compound, v is the linear velocity, D is the gas effective dispersion coefficient and s_i is the source term of each *i* compound. The linear velocity can be assumed to be a function of the drop of pressure in the porous bed according to Darcy's law:

$$v = -k\frac{\partial P}{\partial z} \tag{12}$$

where k is a constant related to the permeability and viscosity of the fluid within the porous bed and z is the longitudinal position in the catalytic bed. Moreover, the variation in the total pressure along the longitudinal position of the PBMR is given not only by this convective transport, but also by the consumption, generation and diffusion of all gaseous compounds. Therefore, the conservation equation for the total pressure is also necessary for the computation:

$$\varepsilon\frac{\partial P}{\partial t} = \frac{\partial}{\partial z}\left(k\frac{\partial P}{\partial z}P\right) + \sum_{i=1}^{n_c} s_i \tag{13}$$

where n_c is the number of compounds.

These equations must be solved for each i compound in both reaction (in the inner tube with the catalytic bed) and permeate sections (in the outer tube) of the membrane reactor. The molar flow rates in a differential reactor portion (dz) are detailed in the diagram of Fig. 2. Please note that the subscripts R and P will be respectively used for referring to the reaction and permeate sections. Then, the convective-dispersive molar transport is quantified by $F_{i,R}$ and $F_{i,P}$, and the source term varies as a function of the section. In the reaction section, the source term ($s_{i,R}$) is defined with two different components: a first one associated to the generation by chemical reaction (molar flow rate Φ_i in Fig. 2) and a second one related to the diffusion of the compounds through the membrane (molar flow rate Ω_i in Fig. 2).

$$s_{i,R} = RT\left(\rho r_i - \frac{4}{d}p_i\Delta P_i\right) \tag{14}$$

where R is the universal gas constant, T is the temperature, r_i is the formation rate of each i compound, ρ is the catalytic bed density, d is the diameter of the inner tube of the

reactor, p_i is the permeance constant of each *i* compound and ΔP_i is the difference between the partial pressures of each *i* compound in the reaction and in the permeate sections.

On the other hand, the source term in the permeate section only considers the diffusion of the compounds from the reaction to the permeate section through the LTA membrane (Fig. 2):

$$s_{i,P} = RT\frac{4}{d}p_i\Delta P_i \tag{15}$$

For the computation, a vector form of Eq. (11) allows for simultaneously modeling the chemical reaction and the deactivation of the catalyst, as previously reported [44]. Thereby, in the reaction section, it takes the form:

$$\varepsilon\frac{\partial(P_R\mathbf{u_R})}{\partial t} = \frac{\partial}{\partial z}\left[vP_R\frac{\partial P_R}{\partial z}\mathbf{u_R} \mp D\frac{\partial(P_R\mathbf{u_R})}{\partial z}\right] + RT\left(\rho\mathbf{r_c} - \frac{4}{d}\mathbf{p}\circ\mathbf{\Delta P}\right) \tag{16}$$

And in the permeate section:

$$\varepsilon\frac{\partial(P_P\mathbf{u_P})}{\partial t} = \frac{\partial}{\partial z}\left[vP_P\frac{\partial P_P}{\partial z}\mathbf{u_P} \mp D\frac{\partial(P_P\mathbf{u_P})}{\partial z}\right] + RT\frac{4}{d}\mathbf{p}\circ\mathbf{\Delta P} \tag{17}$$

Different vectors of variables are introduced in these equations. Please note that the symbol ○ denotes the "element-by-element" multiplication of the vectors. The mixed vectors $\mathbf{u_R}$ and $\mathbf{u_P}$ contain the following dependent variables: a vector $\mathbf{y}_i$ of the molar fraction of each *i* compound and the activity of the catalyst (*a*). In the case of the permeate section, the last position of the vector associated with the catalyst activity takes the value of zero. P_R and P_P are the values of the total pressure in each section. In a similar manner, $\mathbf{r_c}$, $\mathbf{p}$ and $\mathbf{\Delta P}$ are mixed vectors accounting for the formation rate of each *i* compound and deactivation rate, for the permeability of each *i* compound and for the partial pressure gradient between both, respectively.

The matrix-based computation method for solving the system of PDEs is transformed into a system of ODEs by the finite differential method proposed by Skeel and Berzins [45]. And this system of ODEs is integrated using the matrix computation, initial and boundary conditions detailed in the Supporting Information by means of an implicit Runge-Kutta method based on the numerical differentiation formulas of orders 1–5, specific for solving this kind of stiff equations.

3.2. Consideration of the reaction kinetic model

The simultaneous computation of the formation rate of each *i* compound ($\mathbf{r_i}$) and the catalyst deactivation rate (r_d) is allowed because of the definition of the previously introduced vector $\mathbf{r_c}$ in Eq. (16) [44]:

$$\mathbf{r_c} = \begin{bmatrix} \mathbf{r_i} \\ r_d \end{bmatrix} \tag{18}$$

The values of these formation rates are calculated from the reaction rates of each *j* step of the kinetic scheme ($\mathbf{r_j}$) for the direct DME synthesis process (Eqs. (1)-(5)). Defining the mixed vector of reaction and deactivation rates as,

$$\mathbf{r} = \begin{bmatrix} \mathbf{r_j} \\ r_d \end{bmatrix}. \tag{19}$$

The vector of reaction rates is transformed into the vector of formation rates through a coefficient matrix **A**.

$$\mathbf{r_c} = \mathbf{A}\,\mathbf{r} \tag{20}$$

The expression of each reaction rate gathered in the vector $\mathbf{r}_j$ is described in Eqs. (21)-(25), considering the deactivation with the activity parameter (a) [43]. Note that the subscript of each equation coincides with the number of the reactions in Eqs. (1)-(5).

$$r_1 = k_1 \left(P_{CO} P_{H_2}^2 - \frac{P_{CH_3OH}}{K_1} \right) \frac{1}{1+K_{H_2O} P_{H_2O}} a \quad (21)$$

$$r_2 = k_2 \left(P_{CO_2} P_{H_2}^3 - \frac{P_{CH_3OH} P_{H_2O}}{K_2} \right) \frac{1}{1+K_{H_2O} P_{H_2O}} a \quad (22)$$

$$r_3 = k_3 \left(P_{CH_3OH}^2 - \frac{P_{CH_3OCH_3} P_{H_2O}}{K_3} \right) a \quad (23)$$

$$r_4 = k_4 \left(P_{CO} P_{H_2O} - \frac{P_{CO_2} P_{H_2}}{K_4} \right) \frac{1}{1+K_{CO_2} P_{CO_2}} a \quad (24)$$

$$r_5 = k_5 = \beta \quad (25)$$

Each reaction rate is a function of the partial pressure of the reactants and products involved in the reaction step, both related by the thermodynamic equilibrium constant of the reaction. In Eqs. (21)-(24), the reactions are considered to be elemental. The formation rate of CH_4 is assumed to be constant, as the experimental data reveal a low formation of CH_4 independently on the used operation conditions (Eq. (25)). And deactivation rate (r_d) is directly proportional to the partial pressure of the coke precursors (methanol and DME) [20,46]:

$$r_d = -\frac{da}{dt} = k_d \left(P_{CH_3OH} + P_{CH_3OCH_3} \right) \frac{1}{1+K_{d,CO_2} P_{CO_2} + K_{d,H_2O} P_{H_2O}} a \quad (26)$$

The kinetic model of the reaction (Eqs. (21)-(26)) has been previously established in a PBR for this catalyst [43], and the values of the kinetic parameters (kinetic and adsorption equilibrium constants at reference temperature, 275 ºC, activation energies and reaction heats) are listed in Table S2.

3.3. Calculation of the individual permeances

The experiments for determining the individual permeances of the compounds in the reaction medium were conducted in the PBMR under the conditions previously described in Section 2.3. For calculating the values of the *i* compounds permeances (**p**) it has been assumed that these permeances fit a reparameterized exponential tendency with temperature.

$$\mathbf{p} = \mathbf{p}^{*} \circ \exp\left[-\frac{\mathbf{\Delta H_{diff}}}{R}\left(\frac{1}{T^{*}} - \frac{1}{T}\right)\right] \tag{27}$$

where $\mathbf{p}^{*}$ and $\mathbf{\Delta H_{diff}}$ are the vectors of permeances at the reference temperature T^{*} and of the apparent diffusion heats of each *i* compound, respectively.

The values of $\mathbf{p}^{*}$ and $\mathbf{\Delta H_{diff}}$ have been calculated minimizing an objective function (*OF*, Eq. (28)) defined for minimizing the errors between the experimental data $y_{i,R}^{e}$ and $y_{i,P}^{e}$ (molar fractions in the reaction and permeate section, respectively) and those calculated solving the equations of the PBMR model described in section 3.1 and considering the equations and kinetic parameters in sections 3.2 and Table S2, respectively:

$$OF = \sum_{i=1}^{n_c} \omega_i \sum_{n=1}^{n_e} \frac{R_e}{n_e}\left[\left(y_{i,R}^{e} - y_{i,R}\right)^2 + \left(y_{i,P}^{e} - y_{i,P}\right)^2\right]_n \tag{28}$$

where n_c is the number of components, n_e is the total number of experimental data and R_e is the number of repetitions of each experiment. ω_i is the weight factor of each compound, related to the inverse of the variance of each compound according to the expression defined by Constantinides and Mostoufi [47]:

$$\omega_i = \frac{1/\sigma_i^2}{\left[\frac{1}{\sum_{m=1}^{n_v} n_e}\right]\left[\sum_{m=1}^{n_v}\sum_{n=1}^{n_e}\left(1/\sigma_j^2\right)\right]} \tag{29}$$

where σ_i^2 and σ_j^2 are the variances of each curve (distribution of experimental results of compound *i*) in each *j* reaction stage; n_e is the number of experimental points available for each curve; and n_v is the number of dependent variables being fitted.

For the application of the model, along with the equations and kinetic parameters (defined in section 3.2 and Table S2), the SGP* values of Table 1 have been used as initial values to facilitate the calculation.

The calculated individual permeances at the reference temperature (275 ºC, vector $\mathbf{p^*}$) and adsorption heat values (vector $\mathbf{\Delta H_{diff}}$) that offer the best fitting are listed in Table 2.

Table 2. Estimated individual permeances at the reference temperature and adsorption heat values.

Compound	p_i^* (10^{-9} mol m^{-2} s^{-1} Pa^{-1})	$\Delta H_{diff,\,i}$ (kJ mol^{-1})
H_2	39.9	1.68
CO	39.8	1.56
CO_2	40.4	2.38
H_2O	46.3	1.83
MeOH	47.1	3.64
DME	28.5	7.46
HC	40.0	5.00
N_2	40.0	5.00

The H_2O permeance value ($46.3 \cdot 10^{-9}$ mol m^{-2} s^{-1} Pa^{-1}), is close to the lowest limit of the preferred permeability range ($50\text{-}120 \cdot 10^{-9}$ mol m^{-2} s^{-1} Pa^{-1}) reported in the literature by Diban et al. [33] for the synthesis of DME. According to these authors, low H_2O permeability and H_2O/H_2 permselectivity values are preferred to achieve a commitment

between optimal DME and remarkable CO_2 conversion at the described operating conditions. In contrast to the study of Rohde et al. [48] for Fischer-Tropsch synthesis, where high H_2O/H_2 permselectivity is required for achieving high CO_x conversion. Regarding DME permselectivity (H_2O/DME), it is 40 % higher than those of H_2O/H_2 or H_2O/CO. However, the low H_2O/i permselectivity values achieved, explained by the high temperature, reveal the importance of further improving this key property of the membrane. On the other hand, the high computed permeability of methanol was expected. Asides from being a molecule larger than H_2, its polarity favors the absorption onto the zeolite membranes as reported by Salomon et al. [49] using zeolite membranes in the synthesis of MTBE.

4. Validation of the model and simulation of the PBMR

As for qualitatively observing the overall fitting obtained with the model, Fig. S1 shows the parity diagrams for each compound in the reaction section whereas Fig. S2 displays the data in the permeate section. Considering these figures, it can be concluded that the simulation model for the PBMR adjusts appropriately the experimental results, taking into account the experimental complexity as well as the estimation of the parameters above indicated. Both the reaction and the permeate sections are acceptably described with the proposed model. This means that not only the catalyst activity, but also the permeability parameters, are suitable to describe the process performance with the PBMR within a wide range of conditions. The highest relative deviation is observed by the hydrocarbons (Figs. S1g and S2g), nonetheless considering their small concentration, the importance of this compound is insignificant in regards to the rest.

As an example of the model for describing the experimental procedure, Figs. 3 and 4 are presented. These figures show the comparison of the experimental results (symbols) and

those calculated with the PBMR model (lines) for the evolution with time on stream of the compounds molar fractions at the outlet of the reaction (RS, left) and permeate (PS, right) sections. The results in Fig. 3 correspond to a H_2+CO_2 feedstock and 275 ºC for different reaction pressures (20-40 bar) and those in Fig. 4 to a H_2+CO_2 (a and b) and H_2+CO (c) feedstocks at 300 ºC and various pressures. In addition, it is to be highlighted the reduced deactivation of the catalyst in 3 h of time on stream.

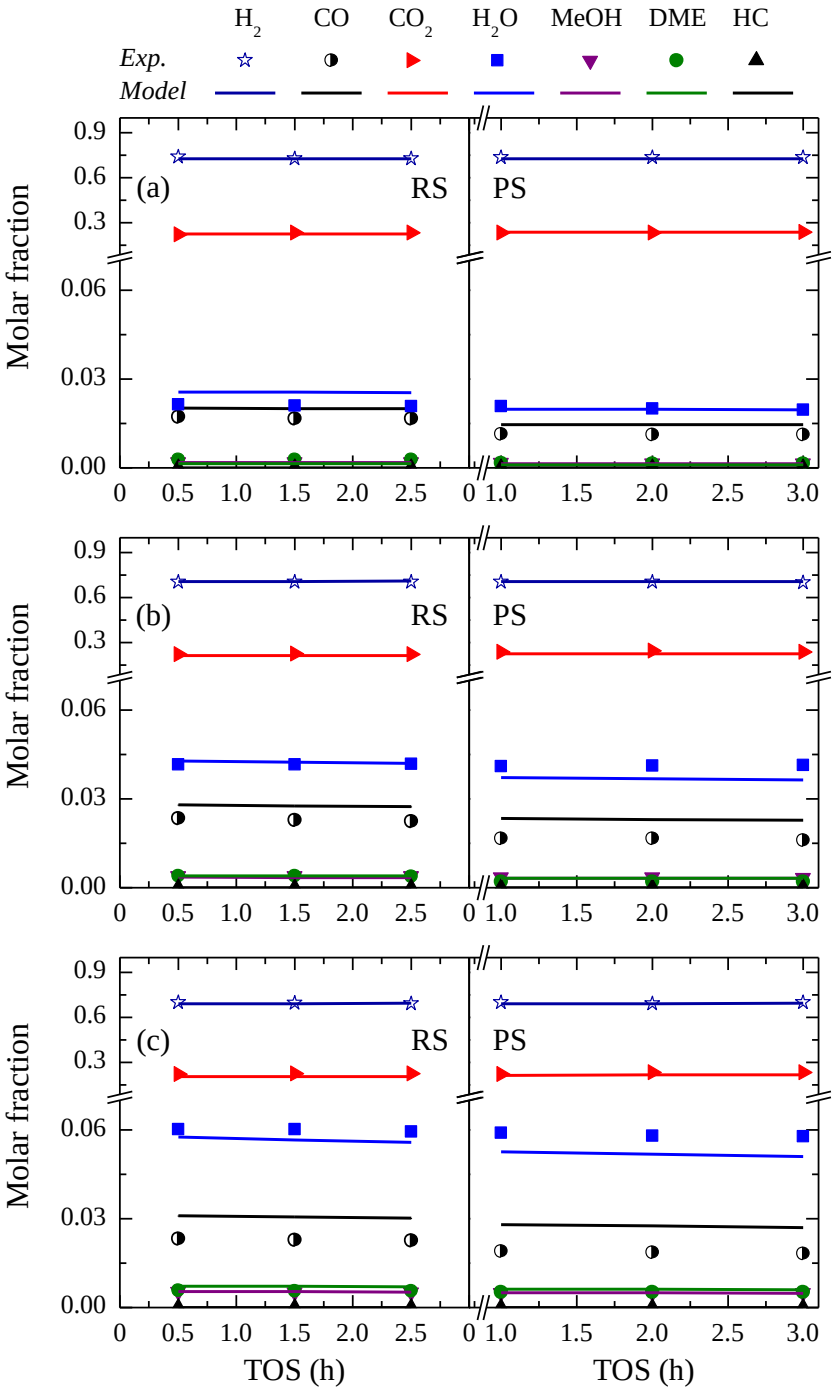

Fig. 3. Comparison of the evolution with time on stream (TOS) of the experimental values of molar fractions (symbols) and those calculated using the PBMR model (lines) in the reaction (left) and permeate (right) sections under 20 bar (a), 30 bar (b) and 40 bar (c). Reaction conditions: feed, H_2+CO_2; 275 ºC; 10 g h $(mol_C)^{-1}$; H_2/CO_x, 3; CO_2/CO_x, 1.

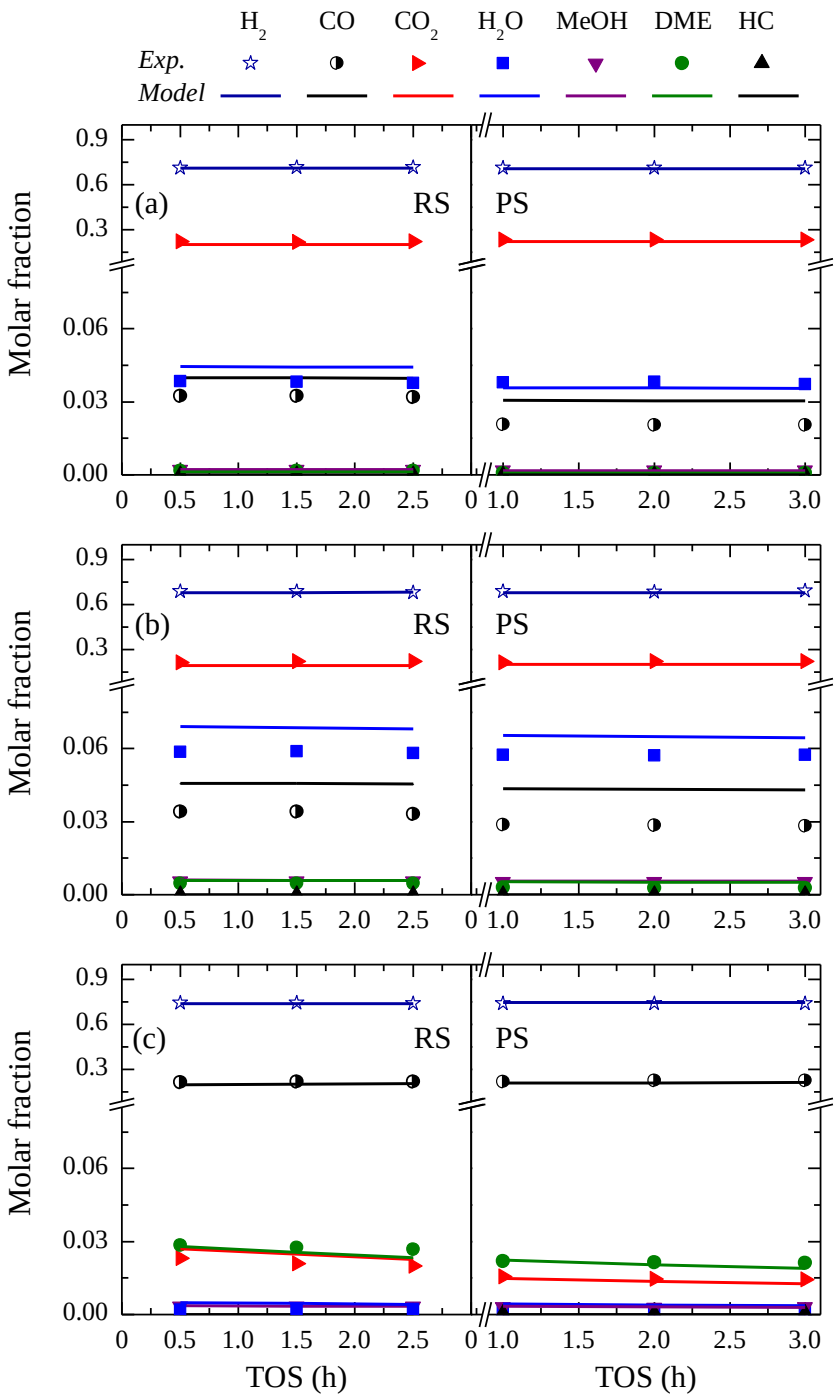

Fig. 4. Comparison of the evolution with time on stream (TOS) of the experimental values of molar fractions (symbols) and those calculated using the PBMR model (lines) in the reaction (left) and permeate (right) sections for CO_2/CO_x, 1 under 20 bar (a) and 40 bar (b); and for CO_2/CO_x, 0 under

40 bar (c). Reaction conditions: feed, H_2+CO_2+CO; 300 ºC; 10 g h $(mol_C)^{-1}$; H_2/CO_x, 3.

As observed, H_2O is the most permeating compound due to the hydrophilic nature of the LTA membrane. Indeed, practically equal concentrations of this compound are detected in both sections of the reactor (reaction and permeate) as theoretically expected. Besides, although in a lower extent, the rest of the compounds do also permeate through the membrane at these temperatures, as it could be expected from the permeation parameters listed in Table 2. In the results in Fig. 4a, the relevant role of H_2O on the catalyst deactivation can be observed. Unlike for H_2+CO_2 feeds (Fig. 3 and Figs. 4a and b), a remarkable decay in DME concentration can be observed for H_2+CO feeds (Fig. 4c). This is a consequence of the higher coke deposition under these conditions, caused by the higher presence of oxygenates in the medium, which are known to be responsible for coke formation in this process [46].

The capacity of the model to predict the macroscopic results such as DME yield or CO_2 conversion is useful and has also been studied. For illustrating the differences between the reaction medium in a PBR and in a PBMR, Fig. 5a shows the comparison of the molar fraction of H_2O in the reaction medium of a PBR with that of the reaction section of the PBMR (in the same reaction conditions as in Fig. 4). Besides, DME yield is also compared for the same conditions (Fig. 5b) to assess the impact of partially removing H_2O from the medium. Comparing the results, H_2O concentration in the reaction section is 6 % lower in the PBMR configuration at 40 bar for CO_2/CO_x ratios in the feed of 1, and 5.8 % lower at 20 bar (Fig. 5a). For syngas feeds, that is, CO_2/CO_x ratio of 0, the difference surpasses 3.5 % (at 40 bar, Fig. 5a). Although these numbers could be interpreted as meaningless, this H_2O removal results in DME yield upgrade up to

64.8 %, 61.5 % and 36.9 %, respectively (Fig. 5b), highlighting the strong influence of the membrane on DME production.

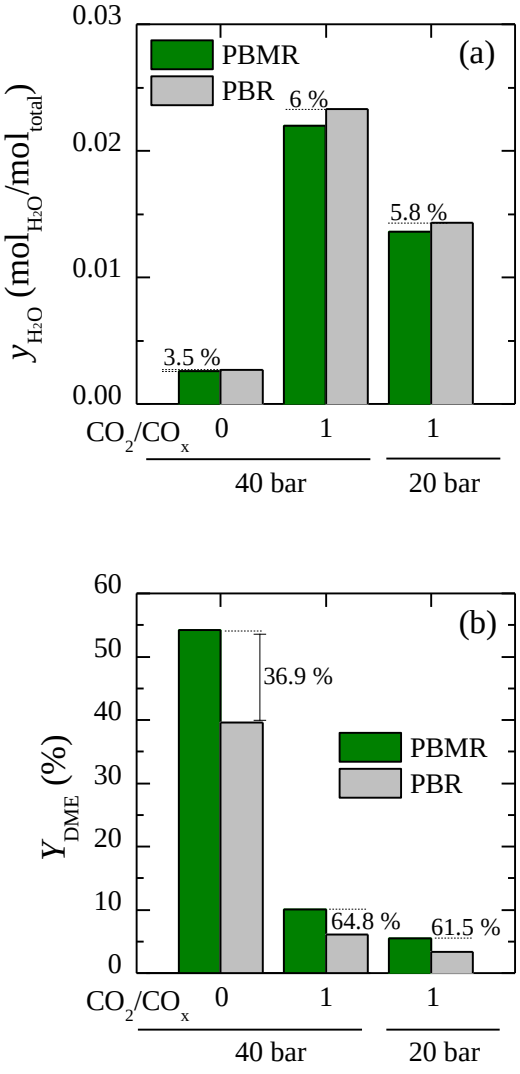

Fig.5. Comparison of the H_2O molar fraction in the reaction section (a) and DME yield (b) at zero time on stream for the PBMR and the PBR. Reaction conditions: 300 ºC; 20 and 40 bar; space time, 10 g h $(mol_C)^{-1}$; H_2/CO_x, 3; CO_2/CO_x, 0 and 1.

In Fig. 6, the evolution with temperature of the experimental DME yields (symbols) are compared to those predicted by the model for the PBMR (continuous lines). These results correspond to 30 bar (Fig. 6a) and 40 bar (Fig. 6b) and in both cases for CO_2/CO_x ratios in the feed of 0, 0.5 and 1. Additionally, on the same graphs the results of the PBR simulation are depicted (dashed lines), to be used as reference for observing the advantage of using the PBMR. This data has been calculated using a kinetic model established in a PBR reactor for the same catalyst, previously reported elsewhere [43]. A good fitting is observed in Fig. 6 between the experimental results of the PBMR and those predicted by the model. These results show the higher yield of DME predicted in the PBMR, where DME yield reaches a 44.4 % at 30 bar and 325 ºC for H_2+CO feeds (Fig. 6a). Increasing reaction pressure to 40 bar boosts this yield to 68.0 % (Fig. 6b). Under these conditions, the increase of DME yield in the PBR is of 35 % (from 31.0 % to 41.9 %). By increasing the CO_2 content in the feed, the DME yield diminishes, and its maximum is found at a lower temperature, 275 ºC for the H_2+CO_2 feed. Likewise, the prediction of methanol yield with the model (Fig. S3) is in accordance with the experimental results, being this yield higher in the PBMR than in the PBR.

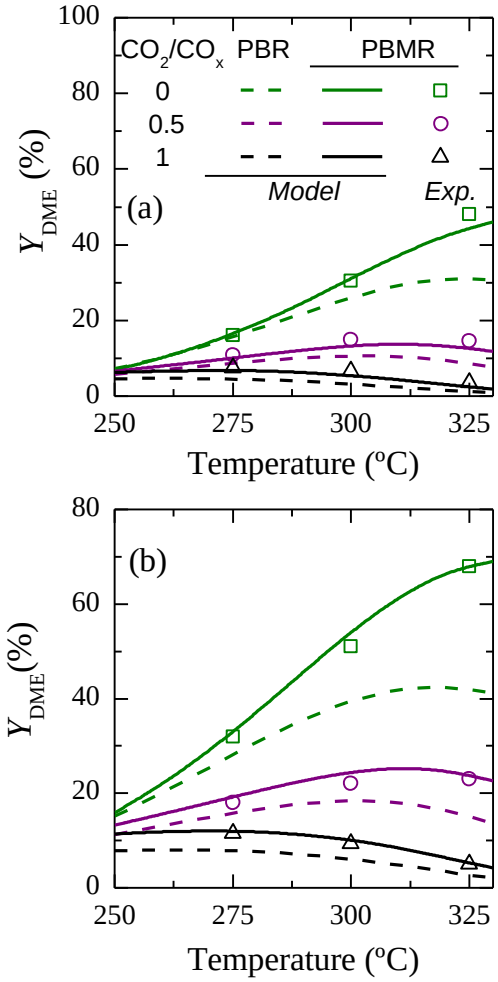

Fig. 6. Evolution with temperature of the DME yields estimated by the model (lines) for the PBMR (continuous) and the PBR (dashed), and the experimental values (symbols) obtained with the PBMR under 30 bar (a) and 40 bar (b). Reaction conditions: space time, 10 g h $(mol_C)^{-1}$; H_2/CO_x, 3; CO_2/CO_x, 0-1.

The calculated and simulation results of the CO_2 conversions evolution with the reaction temperature are compared in Fig. 7 for a CO_2/CO ratio in the feed of 0.5. Similarly to Fig. 6, the results correspond to a space time of 10 g h $(mol_C)^{-1}$. The results

for the simulation of a PBR are also shown. The gain in CO_2 upon increasing temperature is almost linear, achieving values of 16 % at 30 bar and 325 ºC. However, the greatest difference with respect to the PBR is reached at 300 ºC. Based on these results, a DME yield of ca. 24% and a CO_2 conversion of 17% are obtained for H_2+CO+CO_2 feeds with a CO_2/CO_x ratio of 0.5 at 40 bar and 325 ºC.

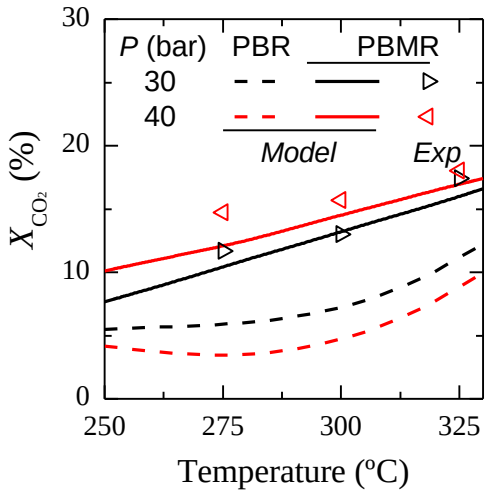

Fig. 7. Evolution with temperature of the CO_2 conversion estimated by the model (lines) for the PBMR (continuous) and the PBR (dashed), and the experimental values (symbols) obtained with the PBMR under 30 bar (a) and 40 bar (b). Reaction conditions: space time, 10 g h $(mol_C)^{-1}$; H_2/CO_x, 3; CO_2/CO_x, 0.5

As an application of the PBMR model to progress towards the development of the PBMR technology, the effect of space time on DME yield (Fig. 8a) and on CO_2 conversion (Fig. 8b) is calculated by maintaining the geometry (length/diameter ratio) of the experimental reactor. The results evidence how the increase in space time, regarding the highest values used in the experiments (10 g h $(mol_C)^{-1}$), allows rising notably DME yield for different values of CO_2/CO_x ratio (Fig. 8a). Furthermore, it is

remarkable that the advantage of the PBMR with respect to the PBR is greater by increasing the space time. The enhancement in DME yield predicted by the model is a consequence of the alteration of the thermodynamic equilibrium that leads to a pseudo-equilibrium state, which will be characteristic of the applied membrane and the reaction and permeation conditions. This greater DME yield *per pass* with a higher space time has a significant impact on the reaction economy, since it will allow reducing the recirculation of the gas flows until achieving an optimal DME yield.

Nevertheless, the increase in space time above 10 g h $(mol_C)^{-1}$ slightly enhances CO_2 conversion for CO_2/CO_x ratios of 0.5 and 1 (Fig. 8b). The superior conversion of CO_2 obtained with the PBMR over the PBR is noteworthy. The extent of the formation of DME in the latter has an unfavorable effect on the conversion of CO_2 because the higher concentration of H_2O favors the formation of CO_2 through the WGS reaction. This situation is avoided in the PBMR with the separation of H_2O from the reaction medium.

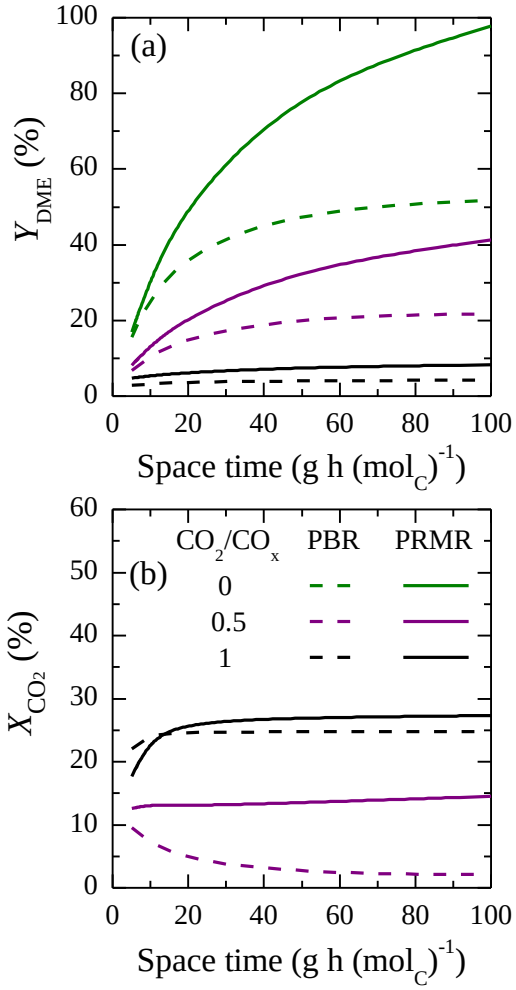

Fig. 8. Evolution with space time of DME yield (a) and CO_2 conversion (b) estimated by the PBMR (continuous) and PBR (dashed) models. Reaction conditions: 30 bar; 325 ºC; H_2/CO_x, 3.

Conclusions

The proposed design model for the direct synthesis of DME in a packed-bed membrane reactor (PBMR), allows predicting the composition of the reaction medium and its evolution over time on stream in a wide range of conditions. The model uses the experimental results of the transport parameters of an LTA membrane and the kinetic model of the CuO-ZnO-ZrO_2/SAPO-11 catalyst.

The PBMR allows obtaining a high yield of DME at higher temperature and space time than with the packed-bed reactor without membrane (PBR) due to the lower thermodynamic limitation. Within the conditions range in which the experimental work has been carried out, with a space time of up to 10 g h $(mol_C)^{-1}$, the simulations predict a higher production of DME with the PBMR. Improvement ranges from 3 % to 5 % in low DME yield conditions (300 ºC and CO_2/CO_x = 1) and from 22 % to 30 % for conditions in which high yield is attained (325 ºC and CO_2/CO_x = 0). A maximum DME yield of 68% is obtained for H_2+CO feeds at 325 ºC and 40 bar, whereas a CO_2 conversion of 17% with a DME yield over 5 % is observed for H_2+CO_2 feeds. The simulation predicts a significant gain in the yield of oxygenates by increasing space time above that experimentally studied, and also a greater difference in this production with respect to that obtained in PBR. The highest DME yield obtained *per pass* will be a significant economic advantage as less intensive recirculation of the unreacted gas stream is required.

Although the use of an inorganic hydrophilic membrane at temperatures up to 325 ºC is a relevant milestone and especially for reaction systems with oxygenates and water, it is to be expected that improvements will be made in the preparation of LTA membranes, and in the selection and preparation of other zeolite membranes with higher H_2O perm-

selectivity and in their future implantation in the reactor. Furthermore, the study of different flow alternatives in the permeate will be interesting, as well as the simulation of the recirculation in order to increase the production of oxygenates or of CO_2 conversion.

Acknowledgements

This work has been carried out with the financial support of the Ministry of Economy and Competitiveness of the Spanish Government (CTQ2016-77812-R), the Basque Government (Project IT1218-19), the ERDF funds and the European Commission (HORIZON H2020-MSCA RISE-2018. Contract No. 823745).

Nomenclature

A	Membrane surface, m^2
a	Activity parameter
D	Gas effective dispersion coefficient, $m^2\ h^{-1}$
d	Reactor diameter, m
$F^0_{CO_2}, F_{CO_2}$	Carbon molar flow rate of CO_2 at the inlet and outlet of the PBMR, $mol_C\ h^{-1}$
$F^0_{CO_x}, F_{CO_x}$	Carbon molar flow rate of the CO + CO_2 mixture at the inlet and outlet of the PBMR, $mol_C\ h^{-1}$
F_i	Carbon molar flow rate of each i compound at the outlet of the reactor, $mol_C\ h^{-1}$

$F_{i,R}$, $F_{i,P}$	Carbon molar flow rate of each *i* compound in the reactor and permeate sections, respectively, $mol_C\ h^{-1}$
K_{CO_2}, K_{H_2O}	Adsorption equilibrium constant related to the attenuation of reaction rate by CO_2or H_2O, respectively, bar^{-1}
K_{d,CO_2}, K_{d,H_2O}	Adsorption equilibrium constant related to the attenuation of deactivation rate by CO_2or H_2O, respectively, bar^{-1}
k	Darcy's law constant, $m^2\ h^{-1}\ bar^{-1}$
k_d	Deactivation kinetic constant, $bar^{-1}\ h^{-1}$
k_j	Kinetic constant of each *j* reaction
K_j	Equilibrium constant of each *j* reaction step of the kinetic scheme
M_i	Total weight of the *i* compound permeate, kg
n_c, n_e, n_i, n_v	Number of compounds in the model, number of experiments , number of carbon atoms in each *i* compound and number of variables being fitted, respectively
OF	Objective function
P, P_i	Total pressure and partial pressure of each *i* compound, bar
P_R, P_P	Total pressures at the reaction and permeate sections, respectively, atm
p_i, p_i^*	Permeance and permeance at the reference temperature of each *i* compound, $mol\ m^{-2}\ h^{-1}\ bar^{-1}$
Q_i	Permeate flux of each *i* compound through the membrane, $kg \cdot m^{-2} \cdot h^{-1}$
R	Universal gas constant
R_e	Number of repetitions of each *n* experimental condition

r_d	Deactivation rate, h^{-1}
r_i	Formation rate of each *i* compound, $mol_C\ g^{-1}\ h^{-1}$
r_j	Reaction rate of each *j* step of the kinetic scheme
$s_{i,R}$, $s_{i,P}$	Source term in the reaction and permeate sections, respectively, bar h^{-1}
T, T^*	Temperature and reference temperature, respectively, K
t	Time, h
X_{CO_2}, X_{CO_x}	CO_2 and $CO+CO_2$ mixture conversions expressed in C units, respectively
Y_i	Yield of each *i* compound expressed in C units
y_{H2O}	Molar fraction of H_2O
y_i,	Molar fraction of each *i* compound expressed in C units
$y^e_{i,R}, y^e_{i,P}$	Experimental molar fraction of *i* compound at *n* experimental condition in the reaction and permeate sections, respectively, expressed in C units
$y_{i,R}, y_{i,P}$	Calculated molar fraction of *i* compound at *n* experimental condition in the reaction and permeate sections, respectively, expressed in C units
z	Longitudinal position in the catalytic bed

Abbreviations

CO_x	$CO + CO_2$ mixture
DME, EtOH, HC, MeOH	Dimethyl ether, ethanol, hydrocarbons and methanol, respectively

PBMR, PBR	Packed bed membrane reactor and packed bed reactor, respectively
PS, RS	Permeation section and reaction section, respectively
TOS	Time on stream, h

Greek symbols

α_i	Separation factor of a binary mixture containing the *i* compound on a membrane
β	Formation rate of hydrocarbons, $mol_C\ g^{-1}\ h^{-1}$
$\Delta H_{diff,i}$	Heat associated with the diffusion through the membrane of each *i* compound, $kJ \cdot mol^{-1}$
ΔP_i	Difference between the partial pressure of compound *i* in the reactor and permeate sections, bar
ε	Effective porosity of the catalytic bed
ρ	Catalyst bed density, $g\ m^{-3}$
σ_i, σ_j	Variances of the experimental results of compound *i* in each *j* reaction stage
v	Gas linear velocity, $m \cdot h^{-1}$
Φi	Carbon molar flow rate of each *i* compound generated by chemical reaction, $mol_C\ h^{-1}$
Ωi	Carbon molar flow rate of each *i* compound through the membrane, $mol_C\ h^{-1}$
ω_i	Weight factor for each *i* compound

Vector and matrices

$\mathbf{\Delta H_{diff}}$	Vector of heats associated with the diffusion through the membrane of each i compound, kJ mol^{-1}
$\mathbf{\Delta P}$	Vector of pressure differences between the reaction and permeate sections for each *i* compound, respectively, bar
A	C balance coefficient matrix
$\mathbf{p}$, $\mathbf{p^*}$	Vectors of permeances and of permeances at the reference temperature of each *i* compound, respectively, mol m^{-2} h^{-1} bar^{-1}
r	Vector containing the reaction rates of each *j* step of the kinetic scheme and the deactivation rate
$\mathbf{r_c}$	Vector containing the reaction rates of each *i* compound and the deactivation rate
$\mathbf{r_i}$	Vector of the formation rates of each *i* compound, mol_C g^{-1} h^{-1}
$\mathbf{r_j}$	Vector of the reaction rates of each *j* step of the kinetic scheme
$\mathbf{u_R}$, $\mathbf{u_P}$	Vector of dependent variables for the reaction and permeate sections, respectively
$\mathbf{y_i}$	Vector of the molar fraction of each *i* compound expressed in C units

REFERENCES

[1] E. Alper, O. Yuksel Orhan, CO_2 utilization: Developments in conversion processes, Petroleum 3 (2017) 109–126. doi:10.1016/j.petlm.2016.11.003.

[2] G. Leonzio, State of art and perspectives about the production of methanol, dimethyl ether and syngas by carbon dioxide hydrogenation, J. CO_2 Util. 27 (2018) 326–354. doi:10.1016/j.jcou.2018.08.005.

[3] A. Rafiee, K. Rajab Khalilpour, D. Milani, M. Panahi, Trends in CO_2 conversion and utilization: A review from process systems perspective, J. Environ. Chem. Eng. 6 (2018) 5771–5794. doi:10.1016/j.jece.2018.08.065.

[4] T.A. Semelsberger, R.L. Borup, H.L. Greene, Dimethyl ether (DME) as an alternative fuel, J. Power Sources 156 (2006) 497–511. doi:10.1016/j.jpowsour.2005.05.082.

[5] C. Arcoumanis, C. Bae, R. Crookes, E. Kinoshita, The potential of di-methyl ether (DME) as an alternative fuel for compression-ignition engines: A review, Fuel 87 (2008) 1014–1030. doi:10.1016/j.fuel.2007.06.007.

[6] P. Pérez-Uriarte, A. Ateka, A.T. Aguayo, A.G. Gayubo, J. Bilbao, Kinetic model for the reaction of DME to olefins over a HZSM-5 zeolite catalyst, Chem. Eng. J. 302 (2016) 801–810. doi:10.1016/j.cej.2016.05.096.

[7] P. Pérez-Uriarte, A. Ateka, A.G. Gayubo, T. Cordero-Lanzac, A.T. Aguayo, J. Bilbao, Deactivation kinetics for the conversion of dimethyl ether to olefins over a HZSM-5 zeolite catalyst, Chem. Eng. J. 311 (2017) 367–377. doi:10.1016/j.cej.2016.11.104.

[8] T. Cordero-Lanzac, A. Ateka, P. Pérez-Uriarte, P. Castaño, A.T. Aguayo, J. Bilbao, Insight into the deactivation and regeneration of HZSM-5 zeolite catalysts in the conversion of dimethyl ether to olefins, Ind. Eng. Chem. Res. 57 (2018) 13689–13702. doi:10.1021/acs.iecr.8b03308.

[9] G.A. Olah, A. Goeppert, G.K.S. Prakash, Chemical recycling of carbon dioxide to methanol and dimethyl ether: From greenhouse gas to renewable, environmentally carbon neutral fuels and synthetic hydrocarbons, J. Org. Chem. 74 (2009) 487–498. doi:10.1021/jo801260f.

[10] W.-H. Chen, C.-L. Hsu, X.-D. Wang, Thermodynamic approach and comparison of two-step and single step DME (dimethyl ether) syntheses with carbon dioxide utilization, Energy 109 (2016) 326–340. doi: 10.1016/j.energy.2016.04.097.

[11] A. Ateka, P. Pérez-Uriarte, M. Gamero, J. Ereña, A.T. Aguayo, J. Bilbao, A comparative thermodynamic study on the CO_2 conversion in the synthesis of methanol and of DME, Energy 120 (2017) 796–804. doi:10.1016/j.energy.2016.11.129.

[12] J. Sun, G. Yang, Y. Yoneyama, N. Tsubaki, Catalysis chemistry of dimethyl ether synthesis, ACS Catal. 4 (2014) 3346–3356. doi:10.1021/cs500967j.

[13] F. Frusteri, M. Migliori, C. Cannilla, L. Frusteri, E. Catizzone, A. Aloise, G. Giordano, G. Bonura, Direct CO_2-to-DME hydrogenation reaction: New evidences of a superior behaviour of FER-based hybrid systems to obtain high DME yield, J. CO_2 Util. 18 (2017) 353–361. doi:10.1016/j.jcou.2017.01.030.

[14] U. Mondal, G.D. Yadav, Perspective of dimethyl ether as fuel: Part I. Catalysis, J. CO_2 Util. 32 (2019) 299–320. doi:10.1016/j.jcou.2019.02.003.

[15] U. Mondal, G.D. Yadav, Perspective of dimethyl ether as fuel_ Part II- analysis of reactor systems and industrial processes, J. CO_2 Util. 32 (2019) 321–338. doi:10.1016/j.jcou.2019.02.006.

[16] A. Ateka, P. Pérez-Uriarte, I. Sierra, J. Ereña, J. Bilbao, A.T. Aguayo, Regenerability of the CuO–ZnO–MnO/SAPO-18 catalyst used in the synthesis of dimethyl ether in a single step, React. Kinet. Mech. Catal. 119 (2016) 655–670. doi:10.1007/s11144-016-1057-y.

[17] G. Bonura, F. Frusteri, C. Cannilla, G. Drago Ferrante, A. Aloise, E. Catizzone, M. Migliori, G. Giordano, Catalytic features of CuZnZr–zeolite hybrid systems for the direct CO_2-to-DME hydrogenation reaction, Catal. Today 277 (2016) 48–54. doi:10.1016/j.cattod.2016.02.013.

[18] M. Sánchez-Contador, A. Ateka, M. Ibáñez, J. Bilbao, A.T. Aguayo, Influence of the operating conditions on the behavior and deactivation of a CuO-ZnO-ZrO_2@SAPO-11 core-shell-like catalyst in the direct synthesis of DME, Renew. Energy 138 (2019) 585–597. doi:10.1016/j.renene.2019.01.093.

[19] G. Bonura, C. Cannilla, L. Frusteri, E. Catizzone, S. Todaro, M. Migliori, G. Giordano, F. Frusteri, Interaction effects between CuO-ZnO-ZrO_2 methanol phase and zeolite surface affecting stability of hybrid systems during one-step CO_2 hydrogenation to DME, Catal. Today 345 (2020) 175–182. doi:10.1016/j.cattod.2019.08.014.

[20] A. Ateka, J. Ereña, J. Bilbao, A.T. Aguayo, Kinetic modeling of the direct synthesis of dimethyl ether over a CuO-ZnO-MnO/SAPO-18 catalyst and assessment of the CO_2 conversion, Fuel Process. Technol. 181 (2018) 233–243.

doi:10.1016/j.fuproc.2018.09.024.

[21] A. Ateka, M. Sánchez-Contador, A. Portillo, J. Bilbao, A.T. Aguayo, Kinetic modeling of CO_2+CO hydrogenation to DME over a CuO-ZnO-ZrO_2@SAPO-11 core-shell catalyst, Fuel Process. Technol. 206 (2020) 106434–106444. doi:10.1016/j.fuproc.2020.106434.

[22] Y. Hu, Z. Nie, D. Fang, Simulation and model design of pipe-shell reactor for the direct synthesis of dimethyl ether from syngas, J. Nat. Gas Chem. 17 (2008) 195-200. doi:10.1016/S1003-9953(08)60051-1.

[23] A.T. Aguayo, J. Ereña, D. Mier, J.M. Arandes, M. Olazar, J. Bilbao, Kinetic modeling of dimethyl ether synthesis in a single step on a CuO-ZnO-Al_2O_3/γ-Al_2O_3 catalyst, Ind. Eng. Chem. Res. 46 (2007) 5522–5530. doi:10.1021/ie070269s.

[24] J. Ereña, I. Sierra, A.T. Aguayo, A. Ateka, M. Olazar, J. Bilbao, Kinetic modelling of dimethyl ether synthesis from (H_2+CO_2) by considering catalyst deactivation, Chem. Eng. J. 174 (2011) 660–667. doi:10.1016/j.cej.2011.09.067.

[25] X. An, Y.Z. Zuo, Q. Zhang, D.Z. Wang, J.F. Wang, Dimethyl ether synthesis from CO_2 hydrogenation on a CuO-ZnO-Al_2O_3-ZrO_2/HZSM-5 bifunctional catalyst, Ind. Eng. Chem. Res. 47 (2008) 6547–6554. doi:10.1021/ie800777t.

[26] V.M.T.M. Silva, C.S.M. Pereira, A.E. Rodrigues, PermSMBR-A new hybrid technology: Application on green solvent and biofuel production, AIChE J. 57 (2011) 1840–1851. doi:10.1002/aic.12381.

[27] M.E.E. Abashar, A.A. Al-Rabiah, Investigation of the efficiency of sorption-

enhanced methanol synthesis process in circulating fast fluidized bed reactors, Fuel Process. Technol. 179 (2018) 387–398. doi:10.1016/j.fuproc.2018.07.028.

[28] N. Diban, A.T. Aguayo, J. Bilbao, A. Urtiaga, I. Ortiz, Membrane reactors for in situ water removal: A review of applications, Ind. Eng. Chem. Res. 52 (2013) 10342–10354. doi:10.1021/ie3029625.

[29] F. Gallucci, L. Paturzo, A. Basile, An experimental study of CO_2 hydrogenation into methanol involving a zeolite membrane reactor, Chem. Eng. Process. Process Intensif. 43 (2004) 1029–1036. doi:10.1016/j.cep.2003.10.005.

[30] D.A. Fedosov, A. V. Smirnov, V. V. Shkirskiy, T. Voskoboynikov, I.I. Ivanova, Methanol dehydration in NaA zeolite membrane reactor, J. Memb. Sci. 486 (2015) 189–194. doi:10.1016/j.memsci.2015.03.047.

[31] J. Gorbe, J. Lasobras, E. Francés, J. Herguido, M. Menéndez, I. Kumakiri, H. Kita, Preliminary study on the feasibility of using a zeolite A membrane in a membrane reactor for methanol production, Sep. Purif. Technol. 200 (2018) 164–168. doi:10.1016/j.seppur.2018.02.036.

[32] I. Iliuta, F. Larachi, P. Fongarland, Dimethyl ether synthesis with in situ H_2O removal in fixed-bed membrane reactor: Model and simulations, Ind. Eng. Chem. Res. 49 (2010) 6870–6877. doi:10.1021/ie901726u.

[33] N. Diban, A.M. Urtiaga, I. Ortiz, J. Ereña, J. Bilbao, A.T. Aguayo, Influence of the membrane properties on the catalytic production of dimethyl ether with in situ water removal for the successful capture of CO_2, Chem. Eng. J. 234 (2013) 140–148. doi:10.1016/j.cej.2013.08.062.

[34] N. Diban, A.M. Urtiaga, I. Ortiz, J. Ereña, J. Bilbao, A.T. Aguayo, Improved performance of a pbm reactor for simultaneous CO_2 capture and DME synthesis, Ind. Eng. Chem. Res. 53 (2014) 19479–19487. doi:10.1021/ie503663h.

[35] M. De Falco, M. Capocelli, A. Basile, Selective membrane application for the industrial one-step DME production process fed by CO_2 rich streams: Modeling and simulation, Int. J. Hydrogen Energy 42 (2017) 6771–6786. doi:10.1016/j.ijhydene.2017.02.047.

[36] M. De Falco, M. Capocelli, A. Giannattasio, Membrane Reactor for one-step DME synthesis process: Industrial plant simulation and optimization, J. CO_2 Util. 22 (2017) 33–43. doi:10.1016/j.jcou.2017.09.008.

[37] A. Ateka, I. Sierra, J. Ereña, J. Bilbao, A.T. Aguayo, Performance of CuO–ZnO–ZrO_2 and CuO–ZnO–MnO as metallic functions and SAPO-18 as acid function of the catalyst for the synthesis of DME co-feeding CO_2, Fuel Process. Technol. 152 (2016) 34–45. doi:10.1016/j.fuproc.2016.05.041.

[38] M. Sánchez-Contador, A. Ateka, P. Rodriguez-Vega, J. Bilbao, A.T. Aguayo, Optimization of the Zr Content in the CuO-ZnO-ZrO_2/SAPO-11 Catalyst for the selective hydrogenation of CO+CO_2 mixtures in the direct synthesis of dimethyl ether, Ind. Eng. Chem. Res. 57 (2018) 1169–1178. doi:10.1021/acs.iecr.7b04345.

[39] M. Sánchez-Contador, A. Ateka, A.T. Aguayo, J. Bilbao, Behavior of SAPO-11 as acid function in the direct synthesis of dimethyl ether from syngas and CO_2, J. Ind. Eng. Chem. 63 (2018) 245–254. doi:10.1016/j.jiec.2018.02.022.

[40] M. Sánchez-Contador, A. Ateka, A.T. Aguayo, J. Bilbao, Direct synthesis of dimethyl ether from CO and CO_2 over a core-shell structured CuO-ZnO-

ZrO_2@SAPO-11 catalyst, Fuel Process. Technol. 179 (2018) 258–268. doi:10.1016/j.fuproc.2018.07.009.

[41] X.M. Liu, G.Q. Lu, Z.F. Yan, J. Beltramini, Recent advances in catalysts for methanol synthesis via hydrogenation of CO and CO_2, Ind. Eng. Chem. Res. 42 (2003) 6518–6530. doi:10.1021/ie020979s.

[42] R.W. Thompson, M.J. Huber, Analysis of the growth of molecular sieve zeolite NaA in a batch precipitation system, J. Cryst. Growth 56 (1982) 711–722. doi:10.1016/0022-0248(82)90056-2.

[43] P. Rodríguez Vega, Experimental development and modeling of a membrane reactor for the direct synthesis of DME with CO_2 valorization, PhD Thesis, University of the Basque Country, UPV/EHU, Bilbao, Spain, 2019.

[44] T. Cordero-Lanzac, A.T. Aguayo, A.G. Gayubo, P. Castaño, J. Bilbao, Simultaneous modeling of the kinetics for n-pentane cracking and the deactivation of a HZSM-5 based catalyst, Chem. Eng. J. 331 (2018) 818–830. doi:10.1016/j.cej.2017.08.106.

[45] R.D. Skeel, M. Berzins, A method for the spatial discretization of parabolic equations in one space variable, SIAM J. Sci. Stat. Comput. 11 (1990) 1–32. doi:10.1137/0911001.

[46] J. Ereña, I. Sierra, M. Olazar, A.G. Gayubo, A.T. Aguayo, Deactivation of a CuO-ZnO-Al_2O_3/γ-Al_2O_3 catalyst in the synthesis of dimethyl ether, Ind. Eng. Chem. Res. 47 (2008) 2238–2247. doi:10.1021/ie071478f.

[47] A. Constantinides, N. Mostoufi, Numerical Methods for Chemical Engineers

with MATLAB Applications, Prentice Hall PTR, New Jersey, 1999, pp. 440-529..

[48] M.P. Rohde, G. Schaub, S. Khajavi, J.C. Jansen, F. Kapteijn, Fischer-Tropsch synthesis with in situ H_2O removal - Directions of membrane development, Microporous Mesoporous Mater. 115 (2008) 123–136. doi:10.1016/j.micromeso.2007.10.052.

[49] M.A. Salomón, J. Coronas, M. Menéndez, J. Santamaría, Synthesis of MTBE in zeolite membrane reactors, Appl. Catal. A Gen. 200 (2000) 201–210. doi:10.1016/S0926-860X(00)00640-2.

Supporting Information for:

Model validation of a packed bed LTA membrane reactor for the direct synthesis of DME from CO/CO_2

Ainara Ateka*, Pablo Rodriguez-Vega, Tomás Cordero-Lanzac, Javier Bilbao, Andrés T. Aguayo

Department of Chemical Engineering, University of the Basque Country UPV/EHU, P.O. Box 644, 48080 Bilbao, Spain

*Corresponding author. Tel.: +34-94-6015361. E-mail address: ainara.ateka@ehu.eus

S1. Catalyst properties

Table S1. Textural, metallic and acid properties of the metallic and acid functions and the catalyst

Property	**CuO-ZnO-ZrO_2**	**SAPO-11**	**CZZr/S-11**
N_2 adsorption-desorption isotherm			
S_{BET} ($m^2\ g^{-1}$)	109	126	122 (60)
$V_{micropore}$ ($cm^3\ g^{-1}$)	0.003	0.037	0.029 (0.014)
$V_{mesopore}$ ($cm^3\ min^{-1}$)	0.267	0.214	0.170 (0.140)
N_2O chemisorption (metallic function)			
S_{Cu} ($m^2\ g_{Cu}^{-1}$)	17.1		53.5 (41.3)**
S'_{Cu} ($m^2\ g_{cat}^{-1}$)	5.9		6.3 (6.1)**
Cu dispersion (%)	2.6		8.2 (6.1)**
NH_3 adsorption-desorption (acid function)			
Total acidity ($mmol_{NH3}\ g^{-1}$)		0.19	0.17 (0.14)
Average acid strength (kJ mol^{-1})		98	85 (72)

**In brackets the value of the catalysts used in reactions under the following conditions: 300 ºC; 30 bar; 10 g·h·$(mol_C)^{-1}$; H_2/CO_x, 3; CO_2/CO_x, 0.5; TOS, 5 h.*

***Properties partially masked by coke deposition.*

S2. Integration method, initial and boundary conditions

The matrix-based calculation method for solving the system of PDEs (each row corresponds to a compound, being the last two ones referred to the catalyst activity and the total pressure) consists of solving in parallel the following matrix system of equation, in the case of the reactor:

$$\begin{pmatrix} \varepsilon P_R & 0 & 0 & \cdots & 0 & \varepsilon y_{\mathrm{H_2},R} \\ 0 & \varepsilon P_R & 0 & & 0 & \varepsilon y_{\mathrm{CO},R} \\ 0 & 0 & \varepsilon P_R & & 0 & \varepsilon y_{\mathrm{CO_2},R} \\ \vdots & & & \ddots & \vdots & \vdots \\ 0 & 0 & 0 & \cdots & 1 & 0 \\ 0 & 0 & 0 & \cdots & 0 & \varepsilon \end{pmatrix} \begin{pmatrix} \frac{\partial y_{\mathrm{H_2},R}}{\partial t} \\ \frac{\partial y_{\mathrm{CO},R}}{\partial t} \\ \frac{\partial y_{\mathrm{CO_2},R}}{\partial t} \\ \vdots \\ \frac{\partial a}{\partial t} \\ \frac{\partial P_R}{\partial t} \end{pmatrix} =$$

$$= \begin{pmatrix} kP_R\left(\frac{\partial P_R}{\partial z}\right) y_{\mathrm{H_2},R} + D\left(\frac{\partial y_{\mathrm{H_2},R}}{\partial z}\right) P_R + RT\rho r_{\mathrm{H_2}} - RT\frac{4}{d} p_{\mathrm{H_2}} \Delta P_{\mathrm{H_2}} \\ kP_R\left(\frac{\partial P_R}{\partial z}\right) y_{\mathrm{CO},R} + D\left(\frac{\partial y_{\mathrm{CO},R}}{\partial z}\right) P_R + RT\rho r_{\mathrm{CO}} - RT\frac{4}{d} p_{\mathrm{CO}} \Delta P_{\mathrm{CO}} \\ kP_R\left(\frac{\partial P_R}{\partial z}\right) y_{\mathrm{CO_2},R} + D\left(\frac{\partial y_{\mathrm{CO_2},R}}{\partial z}\right) P_R + RT\rho r_{\mathrm{CO_2}} - RT\frac{4}{d} p_{\mathrm{CO_2}} \Delta P_{\mathrm{CO_2}} \\ \vdots \\ r_d \\ kP_R\left(\frac{\partial P_R}{\partial z}\right) + RT\rho \sum_i r_i - RT\frac{4}{d}\sum_i p_i \Delta P_i \end{pmatrix} \quad \text{(S1)}$$

And in the permeate section:

$$\left(\begin{array}{ccccc:c:c} P_P & 0 & 0 & \cdots & 0 & y_{\mathrm{H_2},P} \\ 0 & P_P & 0 & & 0 & y_{\mathrm{CO},P} \\ 0 & 0 & P_P & & 0 & y_{\mathrm{CO_2},P} \\ \vdots & & & \ddots & \vdots & \vdots \\ \hdashline 0 & 0 & 0 & \cdots & 1 & 0 \\ \hdashline 0 & 0 & 0 & \cdots & 0 & 1 \end{array}\right) \left(\begin{array}{c} \frac{\partial y_{\mathrm{H_2},P}}{\partial t} \\ \frac{\partial y_{\mathrm{CO},P}}{\partial t} \\ \frac{\partial y_{\mathrm{CO_2},P}}{\partial t} \\ \vdots \\ \frac{\partial a}{\partial t} \\ \frac{\partial P_P}{\partial t} \end{array}\right) =$$

$$= \left(\begin{array}{c} kP_P\left(\frac{\partial P_P}{\partial z}\right) y_{\mathrm{H_2},P} + D\left(\frac{\partial y_{\mathrm{H_2},P}}{\partial z}\right) P_P + RT\frac{4}{d}\, p_{\mathrm{H_2}} \Delta P_{\mathrm{H_2}} \\ kP_P\left(\frac{\partial P_P}{\partial z}\right) y_{\mathrm{CO},P} + D\left(\frac{\partial y_{\mathrm{CO},P}}{\partial z}\right) P_P + RT\frac{4}{d}\, p_{\mathrm{CO}} \Delta P_{\mathrm{CO}} \\ kP_P\left(\frac{\partial P_P}{\partial z}\right) y_{\mathrm{CO_2},P} + D\left(\frac{\partial y_{\mathrm{CO_2},P}}{\partial z}\right) P_P + RT\frac{4}{d}\, p_{\mathrm{CO_2}} \Delta P_{\mathrm{CO_2}} \\ \vdots \\ 0 \\ kP_P\left(\frac{\partial P_P}{\partial z}\right) + RT\frac{4}{d}\sum_i p_i \Delta P_i \end{array}\right) \tag{S2}$$

In order to solve the system of ODEs, after the transformation of the system of PDEs in Eqs. (S1) and (S2), initial and boundary conditions are required. Then, given the three dependent variables $y_i(z,t)$, $a(t)$, and $P(z,t)$, the initial conditions are described as

$$\mathbf{y_i}(z,0) = \mathbf{y_0} \tag{S3}$$

$$a(0) = 1 \tag{S4}$$

$$P(z,0) = P_{in} - \frac{\Delta P_z}{L} z \tag{S5}$$

where $\mathbf{y}_0$ is the vector of molar fractions of each *i* compound at zero time on stream, P_{in} is the pressure at the inlet of the reactor and(ΔP_z) function of the pressure drop along the total length of catalytic bed (L). Please note that the initial conditions are analogous for both reaction and permeate sections in case of molar fractions and pressure. However, in the absence of catalyst, reactions kinetics are not computed in the permeate section and solving the deactivation equation is not required. Therefore, an initial condition for the activity is not necessary.

As the gas linear velocity at the inlet of the reactor is known (v_{in}), Robin and Neumann boundary conditions are used for the molar fraction of each *i* compound:

$$v_{in}\left[\mathbf{y_i}(0,t) - \mathbf{y_0}\right] - D\frac{\partial}{\partial z}\mathbf{y_i}(0,t) = 0 \tag{S6}$$

$$\frac{\partial}{\partial z}\mathbf{y_i}(L,t) = 0 \tag{S7}$$

Due to the absence of dispersion term in the conservation equation for the total pressure, Dirichlet boundary conditions are directly used

$$P(0,t) = P_{in} \tag{S8}$$

$$P(L,t) = P_{in} - \Delta P_z \tag{S9}$$

S3. Matrix of coefficients for the computation of the formation and deactivation rates.

The reaction scheme for the direct synthesis of DME implies the five steps described in Eqs. (1)-(5) of the main manuscript. Taking into consideration the reaction steps stoichiometry, the reaction rate vector and the coefficient matrix

$$\mathbf{r_l} = \begin{pmatrix} r_{H_2} \\ r_{CO} \\ r_{CO_2} \\ r_{H_2O} \\ r_{MeOH} \\ r_{DME} \\ r_{HC} \\ r_d \end{pmatrix} = \begin{pmatrix} -2 & -3 & 0 & 1 & -3 & 0 \\ -1 & 0 & 0 & -1 & -1 & 0 \\ 0 & -1 & 0 & 1 & 0 & 0 \\ 0 & 1 & 1 & -1 & 1 & 0 \\ 1 & 1 & -2 & 0 & 0 & 0 \\ 0 & 0 & 1 & 0 & 0 & 0 \\ 0 & 0 & 0 & 0 & 1 & 0 \\ 0 & 0 & 0 & 0 & 0 & 1 \end{pmatrix} \begin{pmatrix} r_1 \\ r_2 \\ r_3 \\ r_4 \\ r_5 \\ r_d \end{pmatrix} = \begin{pmatrix} -2r_1 - 3r_2 + r_4 - 3r_5 \\ -r_1 - r_4 - r_5 \\ -r_2 + r_4 \\ r_2 + r_3 - r_4 + r_5 \\ r_1 + r_2 - 2r_3 \\ r_3 \\ r_5 \\ r_d \end{pmatrix} \quad \text{(S10)}$$

S4. Kinetic parameters of best fitting for experimental data collected in a PBR configuration

Table S2. Calculated kinetic and adsorption constants at reference temperature (275 ºC), activation energy and adsorption heat values.

Kinetic parameters	Units	Value
k_1^*	$mol_C\ g^{-1}\ h^{-1}\ bar^{-3}$	$5.89 \cdot 10^{-6}$
k_2^*	$mol_C\ g^{-1}\ h^{-1}\ bar^{-4}$	$4.45 \cdot 10^{-7}$
k_3^*	$mol_C\ g^{-1}\ h^{-1}\ bar^{-2}$	$2.57 \cdot 10^{-2}$
k_4^*	$mol_C\ g^{-1}\ h^{-1}\ bar^{-2}$	$2.86 \cdot 10^{0}$
β	$mol_C\ g^{-1}\ h^{-1}$	$4.24\ 10^{-7}$
E_1	$kJ\ mol^{-1}$	$8.54 \cdot 10^{1}$
E_2	$kJ\ mol^{-1}$	$5.44 \cdot 10^{1}$
E_3	$kJ\ mol^{-1}$	$5.52 \cdot 10^{1}$
E_4	$kJ\ mol^{-1}$	$5.06 \cdot 10^{1}$
$K^*_{H_2O}$	bar^{-1}	$3.40 \cdot 10^{0}$
$K^*_{CO_2}$	bar^{-1}	$2.63 \cdot 10^{-1}$
ΔH_{H_2O}	$kJ\ mol^{-1}$	$9.29 \cdot 10^{-2}$
ΔH_{CO_2}	$kJ\ mol^{-1}$	$8.16 \cdot 10^{-2}$
k_d^*	$h^{-1}\ bar^{-1}$	$1.31 \cdot 10^{-1}$
E_d	$kJ\ mol^{-1}$	$2.74 \cdot 10^{-1}$
K^*_{d,H_2O}	bar^{-1}	$1.32 \cdot 10^{-2}$
K^*_{d,CO_2}	bar^{-1}	$1.27 \cdot 10^{-2}$
$\Delta H_{d,H_2O}$	$kJ\ mol^{-1}$	$5.36 \cdot 10^{-1}$
$\Delta H_{d,CO_2}$	$kJ\ mol^{-1}$	$1.36 \cdot 10^{0}$
Error		$3.74 \cdot 10^{-3}$
Residual variance		$3.76 \cdot 10^{-5}$

S5. Model validation with experimental data

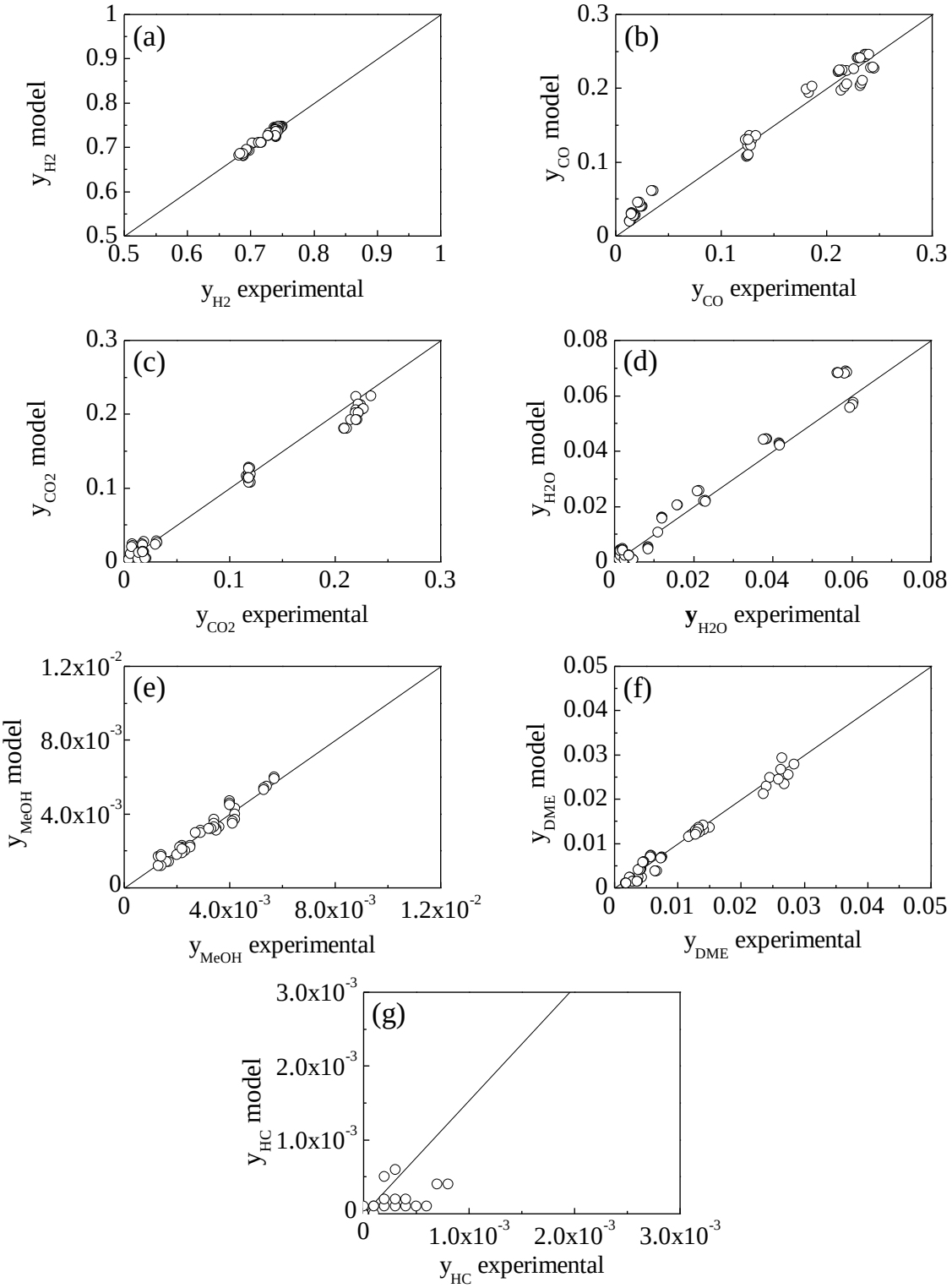

Fig. S1. Fitting of the experimental values of products molar fractions to those calculated with the PBMR model in the reaction section. H_2 (a), CO (b), CO_2 (c), H_2O (d), MeOH (e), DME (f) and N_2 (g).

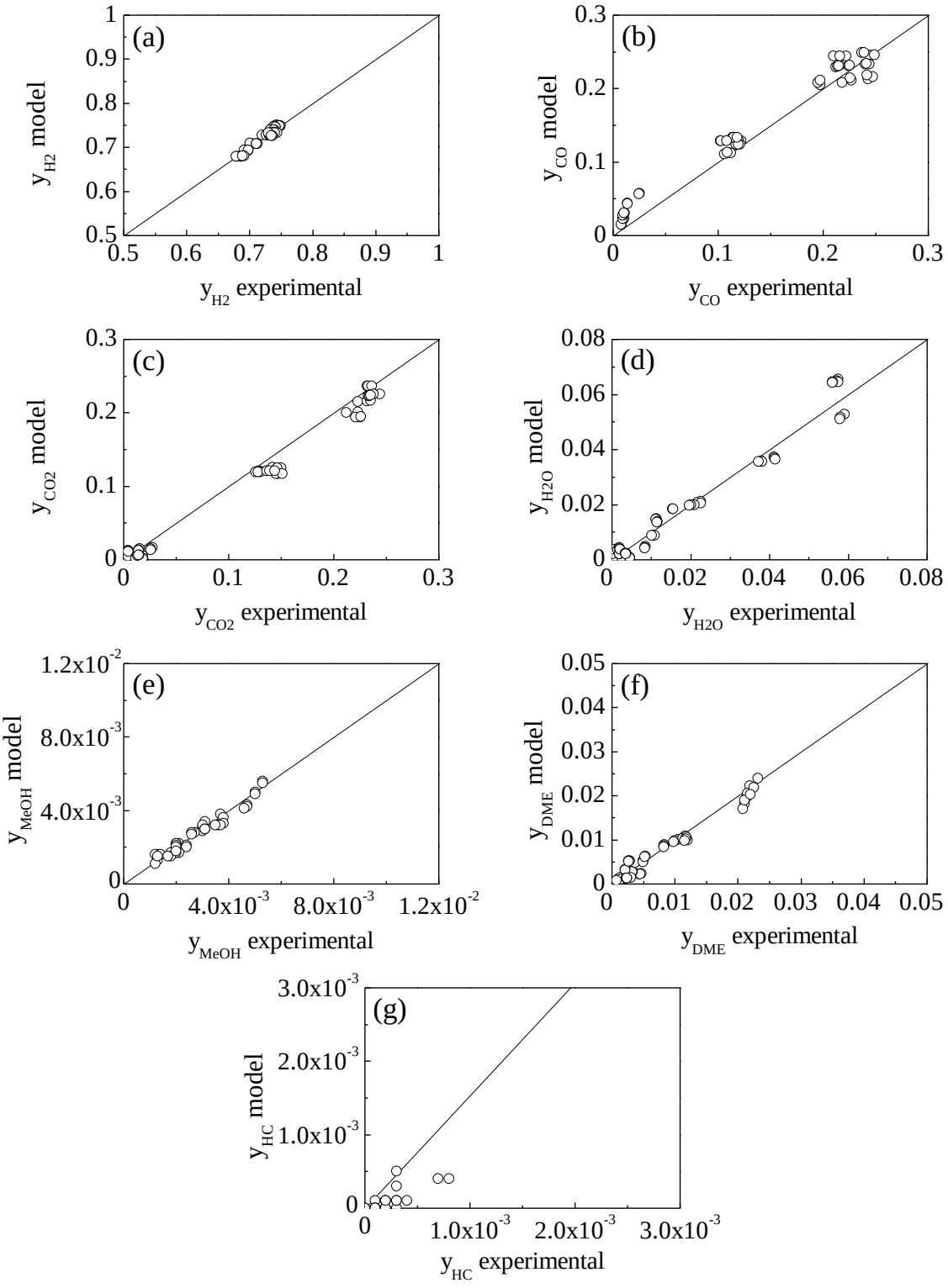

Fig. S2. Fitting of the experimental values of products molar fractions to those calculated with the PBMR model in the permeate section. H_2 (a), CO (b), CO_2 (c), H_2O (d), MeOH (e), DME (f) and N_2 (g).

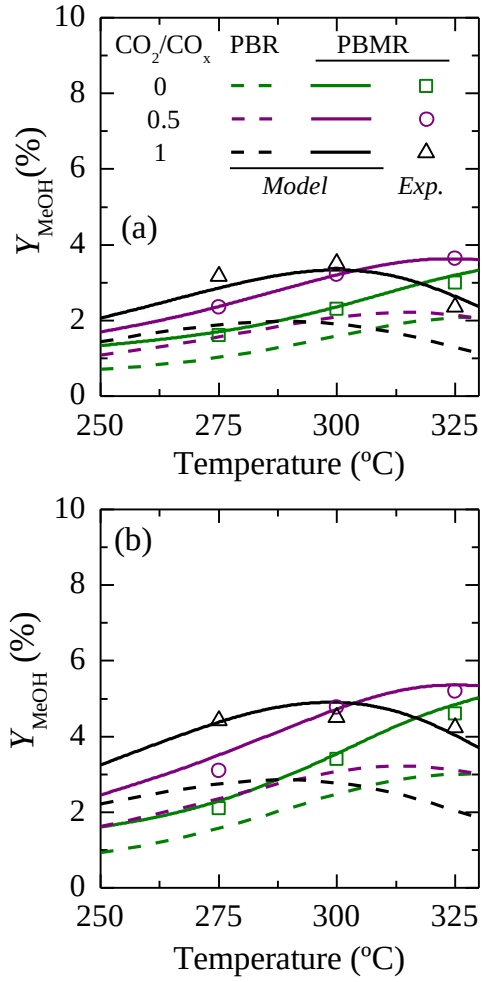

Fig. S3. Evolution with temperature of the MeOH yield estimated by the model (lines) for the PBMR (continuous) and PBR (dashed), and the experimental values (symbols) obtained with the PBMR under 30 bar (a) and 40 bar (b). Reaction conditions: space time, 10 g h $(mol_C)^{-1}$; H_2/CO_x, 3; CO_2/CO_x, 0-1.

Additional nomenclature

E_j	Activation energy of each *j* step of the kinetic scheme, kJ mol^{-1}
E_d	Activation energy of deactivation, kJ mol^{-1}
$K^*_{d,CO_2}, K^*_{d,H_2O}$	Adsorption equilibrium constant at reference temperature related to the attenuation of deactivation rate by CO_2 or H_2O, respectively, bar^{-1}
$K^*_{CO_2}, K^*_{H_2O}$	Adsorption equilibrium constant at reference temperature related to the attenuation of reaction rate by CO_2 or H_2O, respectively, bar^{-1}
k_d^*	Deactivation kinetic constant at the reference temperature, respectively, $atm^{-1}\ h^{-1}$
k_j^*	Kinetic constant of each *j* step of the kinetic scheme at the reference temperature
L	Reactor bed length, m
P_{in}	Pressure at the inlet of the reactor, bar
S_{Cu}, S'_{Cu}	Cu surface area expressed as $m^2\ g_{Cu}^{-1}$ and $m^2\ g_{cat}^{-1}$, respectively
S_{BET}	BET specific surface area, respectively, $m^2\ g^{-1}$
$V_{mesopore}$, $V_{micropore}$	Mesopore and micropore volume, respectively, $cm^3\ g^{-1}$
$\mathbf{y_0}$	Vector of the initial molar fractions of each *i* compounds expressed in C units
ΔH_i, $\Delta H_{d,i}$	Adsorption heat of each *i* compound related to the attenuation of the reaction and deactivation rates, respectively, kJ mol^{-1}
ΔP_z	Pressure drop along the length of the catalytic bed, bar
v_{in}	Gas linear velocity at the inlet of the PBMR, m h^{-1}